Rectifiers, MOS diodes and LEDs made of fully porous GaN produced by Chemical Vapor Deposition

J. J. Carvajal,[a,*] J. Mena,[a] J. Aixart,[a] C. O'Dwyer,[b] F. Díaz,[a] and M. Aguiló[a]

[a]Física i Cristal·lografia de Materials i Nanomaterials, FiCMA-FiCNA, and EMaS, Dept. Química Física i Inorgànica, Universitat Rovira i Virgili, URV, Marcel·lí Domingo 1, E-43007, Spain
[b]Department of Chemistry, University College Cork, Cork, Ireland

Here we present the fabrication of LEDs based on porous GaN produced by chemical vapor deposition (CVD) and reviewed the work done that allowed demonstrating *p-n* junction rectifiers and MOS diodes in a simple manner and without involving post-growth steps to induce porosity. *p-n* junction rectifiers exhibited stable rectification in the range ±1-±5 V, with very stable values of current with time. MOS diodes were fabricated in a single growth step formed by a MgO dielectric interlayer in between Mg-doped porous GaN and a Mg-Ga metallic alloy. Despite the high resistivity observed in the LEDs fabricated, that induced a turn on voltage of ~13 V, the emission consisted only in one peak centered at 542 nm. Our porous GaN films exhibit random porosity when compared to arrays of nanostructures, however, their easy deposition over large areas without dominating leakage currents is promising for wideband gap applications.

Introduction

GaN is a hexagonal semiconductor, crystallizing in the space group $P6_3mc$ with the wurtzite structure (1). It is considered an important wide band-gap semiconductor for a good number of applications in electronics and optoelectronics (2). It possess a large band gap, that together with its thermal stability and excellent physical properties, make of GaN an excellent candidate for high temperature electronics (3). From another side, GaN exhibits a high heat capacity and a high thermal conductivity, which makes it suitable for high power and high frequency applications (4). Its high stability in front ionizing radiations makes it also good for applications in space, betavoltaics and photovoltaics (5-6).

In its porous form, GaN is particularly interesting for developing optoelectronic devices with improved efficiency, such as LEDs with enhanced efficiency (7-15) and sensors with enhanced sensitivity (16-17). It has also been demonstrated that porous GaN exhibits a reduced structural stress when compared to its non-porous form (18). Despite not being as popular as its bulk counterpart is, the interest in porous GaN has been maintained since the first references in which it was reported, back in 1999, as can be seen in Figure 1, with a tendency to increase the number of papers published about this subject as the time goes by.

Porous GaN is produced typically by (photo)electrochemical etching and chemical etching methods (19-22). An alternative to produce porous GaN we proposed some time ago is the chemical vapour deposition (CVD) method (23), through which we have shown that it is possible to produce nanoporous GaN without any etching or chemical post-growth treatment, with the porosity being present only on the (0001) face of the material. By using this technique, we have demonstrated that it is possible to form low resistivity Ohmic Pt and Au metallic contacts on porous *n*-type GaN by the formation of intermetallic seed layers through the vapour-solid-solid (VSS) mechanism (24). Also, we have been able to develop *p*-type porous GaN by doping it with Mg, with a charge carrier concentration of the order of 10^{18} cm^{-3} (25). By tuning the concentration of Mg, introduced as Mg_2N_3 in the CVD system, we have shown that it is possible to form a polycrystalline high-κ oxide between an Ohmic metallic alloy interlayer contact and the porous GaN, while maintaining a clean interface, that allowed to fabricate MOS-type diodes on silicon substrates in a single growth step (26). Besides, through the careful selection of the substrate it has also been possible to produce porous GaN epitaxial layers (27-28) that allow for the fabrication of high quality partially and fully porous GaN rectifying *p*-*n* junctions, through a two step CVD process, and show their behaviour as diodes with effective uniform conduction under a green technology (29).

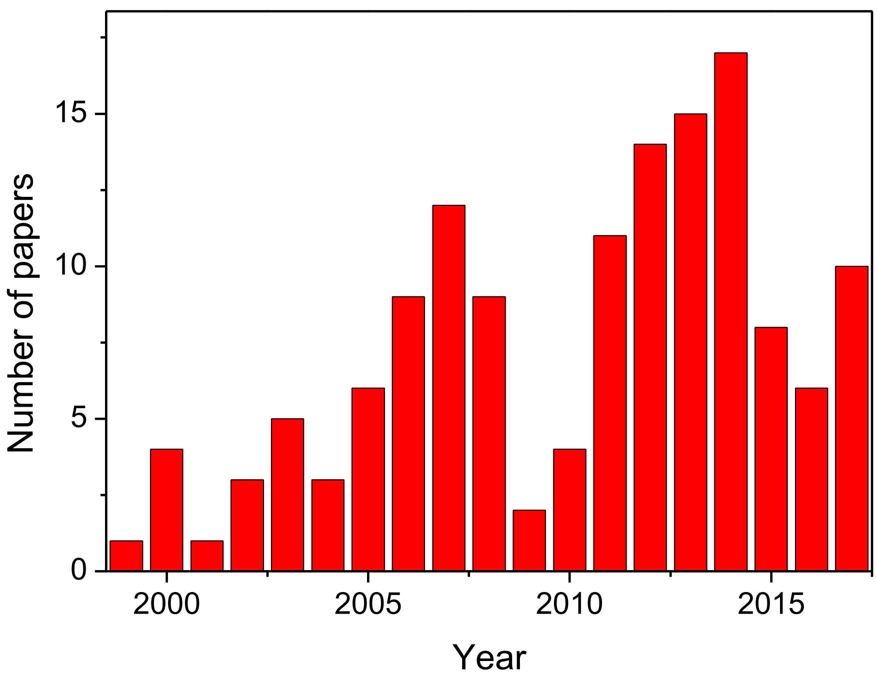

Figure 1. Number of papers published per year since 1999 about porous GaN (Source: Scopus).

Here, we review the work we have done in porous GaN in the recent years, and present also the promising results we obtained in the light emission of these structures. Thus, we are convinced that these porous *p*-*n* junctions have potential applications in rectifiers' technology, high power diodes, LEDs with enhanced light emitting properties and high surface area sensors with improved sensitivity.

Porous GaN rectifiers fabricated by CVD

CVD growth and morphological characterization

Porous GaN layers have been grown on non-porous GaN films (~ 5 µm thick) on sapphire with *n*-type or *p*-type conductivity, depending on the experiment and the *p-n* junction to be formed. For that we used the direct reaction between Ga and NH_3 in a CVD system (28). Mg_3N_2 was used as the Mg source, located upstream of the Ga source (30). The substrates were placed above the Ga source at a vertical distance of 1.7 cm. Once the substrates and the Ga and Mg precursors, when needed, were introduced in the furnace, the reactor was degassed to 1×10^{-2} Torr, prior to the introduction of NH_3 at a constant flow rate of 75 sccm. Figure 2 shows a scheme of the CVD growth setup used. During the reaction, that lasted for 60 min, the pressure of the system was set at 15 Torr, while the reaction was kept at 930 ºC. To stop the synthesis process, the ammonia flow was shut down and the temperature was decreased to room temperature. To select and control the areas of the substrate on which the porous GaN layers were deposited, a selective-area growth process was used, covering the substrate with a BN mask. Finally, to activate the *p*-type conductivity of the Mg-doped samples, we annealed them at 700 ºC in a nitrogen atmosphere during 20 min.

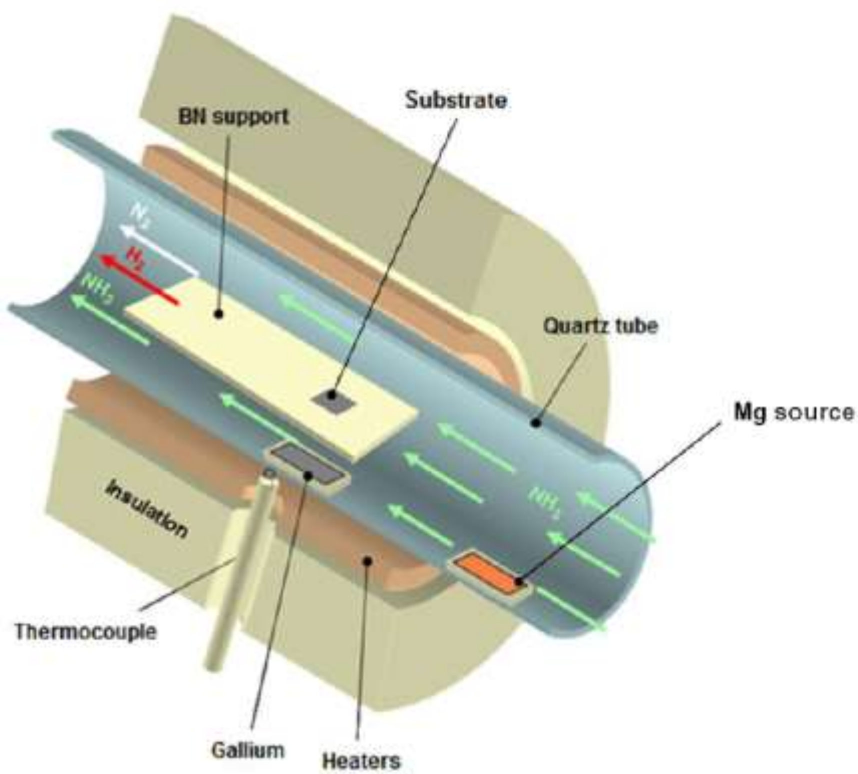

Figure 2. Schematic representation of the CVD system used for the growth of porous GaN layers.

Three types of porous GaN diodes were prepared: (i) undoped *n*-type porous GaN grown on non-porous *p*-type GaN; (ii) Mg-doped porous *p*-type GaN grown on non-porous *n*-type GaN; and (iii) Mg-doped porous *p*-type GaN grown on undoped porous *n*-type GaN previously grown on non-porous *n*-type GaN (28). The last type of diodes were grown on a two crystal growth step process. In the first step, an undoped *n*-type porous GaN film was grown on a non-porous GaN substrate with (0001) crystallographic orientation. Then, the porous Mg-doped *p*-type GaN layer was grown on the top of this undoped porous GaN film.

The SEM images recorded for the porous layers obtained reveal a high degree of porosity. However, the diameters of the pores tend to be slightly bigger in the Mg-doped samples when compared to those of the undoped samples. This is even more evident when we compare the diameters of the pores of the two layers constituting the fully porous GaN diode, i.e. the one formed by a Mg-doped porous *p*-type GaN layer grown on an undoped porous *n*-type GaN layer previously deposited on a non-porous *n*-type GaN substrate, as can be seen in Figure 3. This might be due to the exposure of this sample at high temperatures during a longer time. This would widen the pores by a thermal etching effect (31). Another reason that might contribute to the widening of the pores would be their corrugation during the second growth step (32).

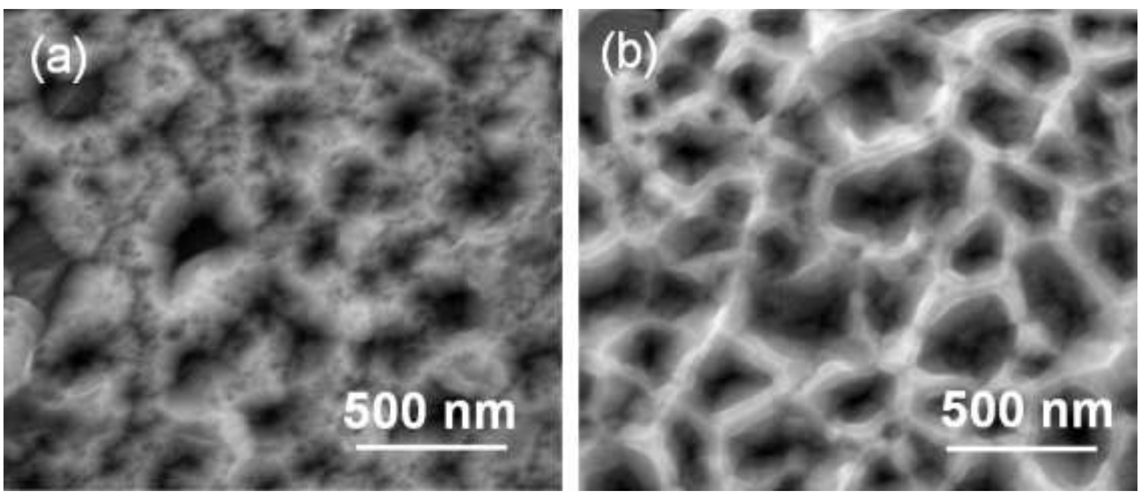

Figure 3. High magnification SEM images of the porous structures observed on (a) *n*-type and (b) Mg-doped GaN layers corresponding to the type (iii) diode, i.e. a Mg-doped porous *p*-type GaN layer grown on an undoped porous *n*-type GaN layer previously deposited on a non-porous *n*-type GaN substrate.

An important aspect to be mentioned is that in all cases, the porous GaN layers grew crystallographically oriented along the *c* direction, matching the crystallographic direction provided by the substrates used.

This was revealed by the rocking curves corresponding to the $(10\bar{1}2)$ and (0004) reflections of the porous layers. The rocking curves were recorded using a Bruker-AXS D8-Discover diffractometer equipped with a parallel incident beam (Göbel mirror), a vertical θ-θ goniometer, an XYZ motorized stage, and a General Area Diffraction Detection System (GADDS) HI-STAR detector with a multiwire proportional counter of 30×30 cm^2 area and 1024×1024 pixel density. Samples were placed on the sample holder fixed with wax, and the area of interest was selected with the aid of a video-laser focusing system. An X-ray collimator system allows the analysis of an area of 500 μm^2

on the sample. The X-ray diffractometer was operated at 40 kV and 20 mA. For this purpose, the X-ray source and the X-ray detector positions were settled at the desired Bragg angle, corresponding to the particular reflection of interest, and 120 frames were recorded at an integration time of 1 s every 0.05º in ω. The ω-scan was set to start at an ω angle 3º below the desired Bragg angle, and was finished 3º above that Bragg angle. The envelope function of the collection of 120 frames was then plotted, obtaining the corresponding rocking curve. For the identification of the $(10\bar{1}2)$ peak a χ- and a ϕ-scan were performed to identify the right diffraction conditions. The χ-scan was fixed when the k vector was perpendicular to the $(10\bar{1}2)$ plane. This χ angle was defined using the stereographic projection and measuring the angle between the $(10\bar{1}2)$ and (0001) planes. Then, a ϕ-scan was recorded to find the location of the *a* (or *b*) crystallographic axis. This procedure allowed identifying peaks that are off the plane of the sample when the thin film was parallel to the ground platform. For this, the X-ray source and the detector were positioned at a defined θ Bragg angle and then, the sample was rotated in 5 degrees steps 36 times with an integration time of 5 seconds, covering an angle of 180º in ϕ. Once the ϕ angle was roughly identified following these conditions, a second ϕ-scan was performed to found more accurately its value, using 1 degree steps 5 times with an integration time of 5 seconds. Once the ϕ and χ angles were defined the rocking curves were recorded, with an initial ω_1 = 21.19º and a final ω_2 = 27.19º for the $(10\bar{1}2)$ reflection, and an initial ω_1 = 33.44º and a final ω_2 = 39.44º for the (0004) reflection. Figure 4 shows a scheme of how the rocking curves were recorded.

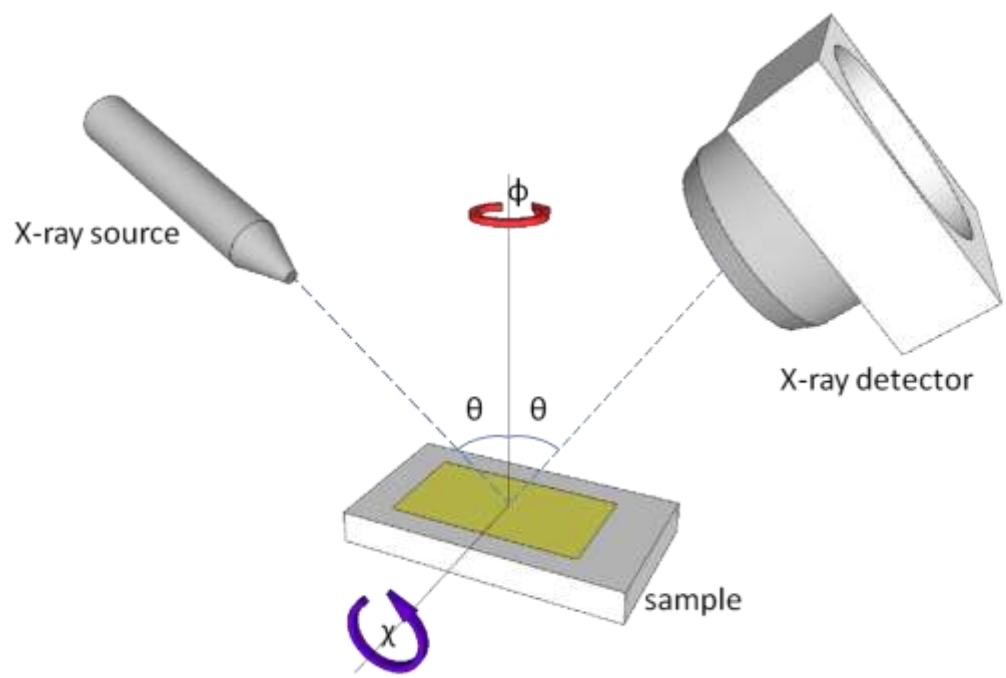

Figure 4. Schematic representation of the ϕ, χ and θ (ω) rotations used to record the rocking curves in the porous GaN samples.

As an example, Figure 5 shows the rocking curve corresponding to the undoped porous GaN layer. From the data extracted from the figure, the position and the full width at half-maximum (FWHM) of the diffraction peaks of the porous layer could be analyzed.

Table 1 lists these data. The FWHM of the rocking curves are similar in both cases, indicating a good structural quality for the porous layer. In fact, for the non-porous substrate, similar values were obtained, indicating that the structural quality of the porous layer is at least as good as that of the commercial substrates.

TABLE I. Peak position and FWHM of the rocking curves shown in Figure 5 recorded for porous GaN.

Reflection	Peak position (º)	FWHM (º)
$(10\bar{1}2)$	25.54	0.15
(0004)	37.01	0.15

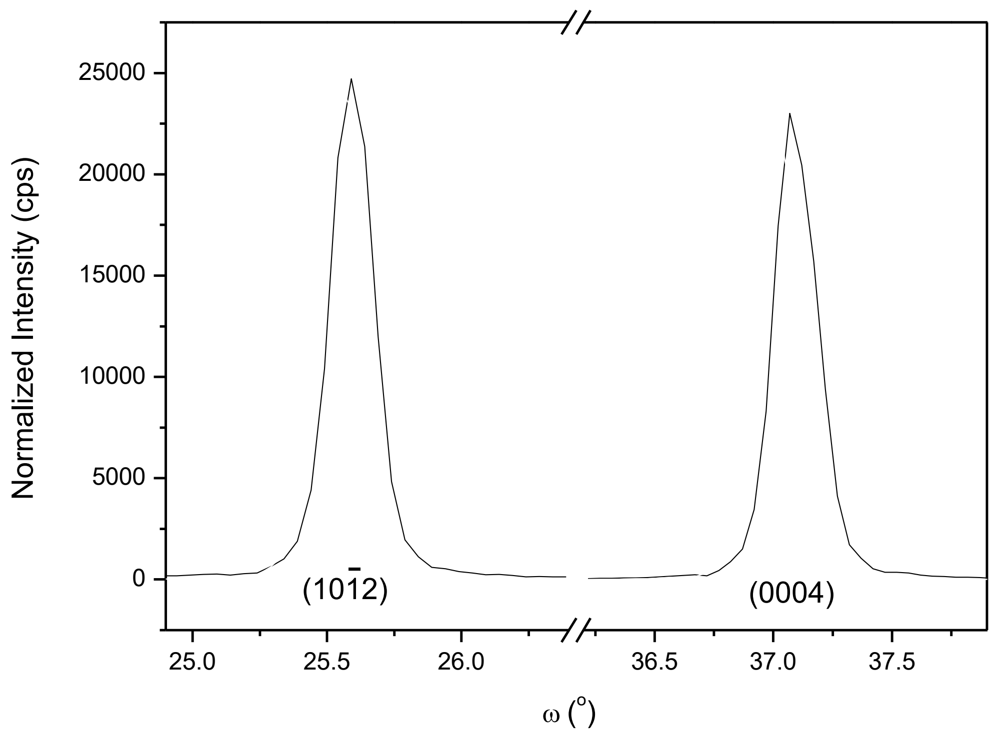

Figure 5. Rocking curves corresponding to the $(10\bar{1}2)$ and (0004) reflections of an undoped porous GaN grown on a non-porous *p*-type GaN substrate.

Electrical characterization

Electrical characterization of the three different types of porous GaN diodes fabricated was performed using the two-probe electrical measurements technique. As contacts we used In/Ga liquid drops placed on the top of the porous GaN layer and the non-porous GaN substrate, in the case of the diodes formed by an undoped *n*-type porous GaN layer grown on non-porous *p*-type GaN substrates or by a Mg-doped porous *p*-type GaN layer grown on non-porous *n*-type GaN substrates, to ensure a good wetting area of several μm^2 to the rough top-surface of the porous GaN samples. In the case of the Mg-doped porous *p*-type GaN layer grown on an undoped porous *n*-type GaN film previously grown on a non-porous *n*-type GaN substrate, the In/Ga liquid drops were placed on the top of the two porous layers. For the measurements, a Keithley 2400 sourcemeter was used. Linear voltage sweeps were obtained in the range between -10 and 10 V with a 50 mV/s sweep rate. The measurements were repeated with contacts on various points of each sample to ensure repeatability.

Figure 6 shows the I-V curves recorded for a diode formed by an undoped *n*-type porous GaN layer grown on the top of a non-porous *p*-type GaN substrate. All the samples exhibited characteristic I-V curves with strong rectification (28). From these curves we found that the barrier to the exponential current increase was lower than the expected GaN diode response, happening below 1 V at around 05-0.68 V, in the $(E_g/4q)$ – $(E_g/2q)$ range. Figure 5(a) shows the I-V curves recorded in several locations of the same diode, showing the homogeneity in the electrical behavior of the devices. Figure 6(b) shows the I-V curves recorded for 25 different diodes. In this case, despite the current obtained at +3 V for the different devices varies between 6 and 10 mA, the knee voltage is located in the range 0.5-0.68 V in all cases, indicating the good reproducibility of this technique for the fabrication of porous GaN diodes.

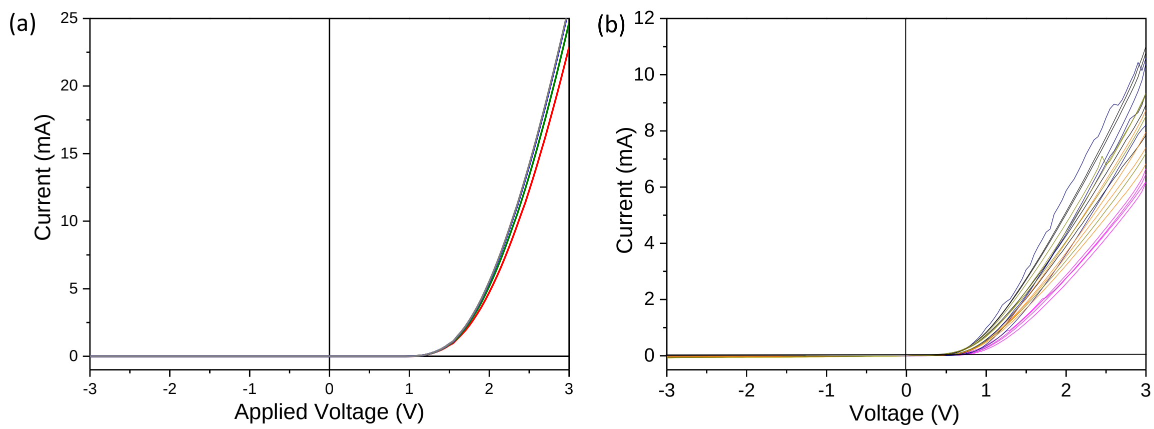

Figure 6. I-V curves recorded for a diode formed by an undoped *n*-type porous GaN layer grown on the top a non-porous *p*-type GaN substrate. (a) I-V curves recorded on different points of the same diode, and (b) I-V curves recorded for different diodes.

An important property of a *p-n* junction is the rectifying effect, which means that it only allows the electric current to flow in one direction. Diode rectification measurements were conducted in the range between -0.4 and +0.4 V, and -5 V and +5 V voltages for forward and reverse bias, respectively. As expected, by applying both reverse and forward bias to the porous GaN diodes, a distinct rectifying behavior was observed (28). Figure 7 shows current vs. time plots recorded at different constant voltages for each of the three porous GaN diodes, after changing the polarity of diode bias with a frequency of 0.1 Hz. All diodes exhibited stable rectification. The I-t characteristics recorded at ±0.4 V does not show clear rectification behavior, since this voltage is below the turn-on voltage of the porous GaN diodes. At ±1 V, ±2 V, ±3 V and ±5 V voltages all diodes demonstrate rectifying behavior. The highest leakage voltage and the lowest rectification ratio were observed at ±5 V. Also, porous GaN diodes demonstrate very stable values of current with time at both, forward and reverse bias. The stability confirms that for porous *p-n* junctions using a single porous layer deposited on an epitaxial continuous GaN film, or from a porous layer grown on another porous layer, a remarkable stability in rectification is maintained. Porous GaN films can exhibit random porosity (compared to arrays of nanostructures), but their ease of deposition over large areas without dominating leakage currents is promising for wideband gap applications, including sensors.

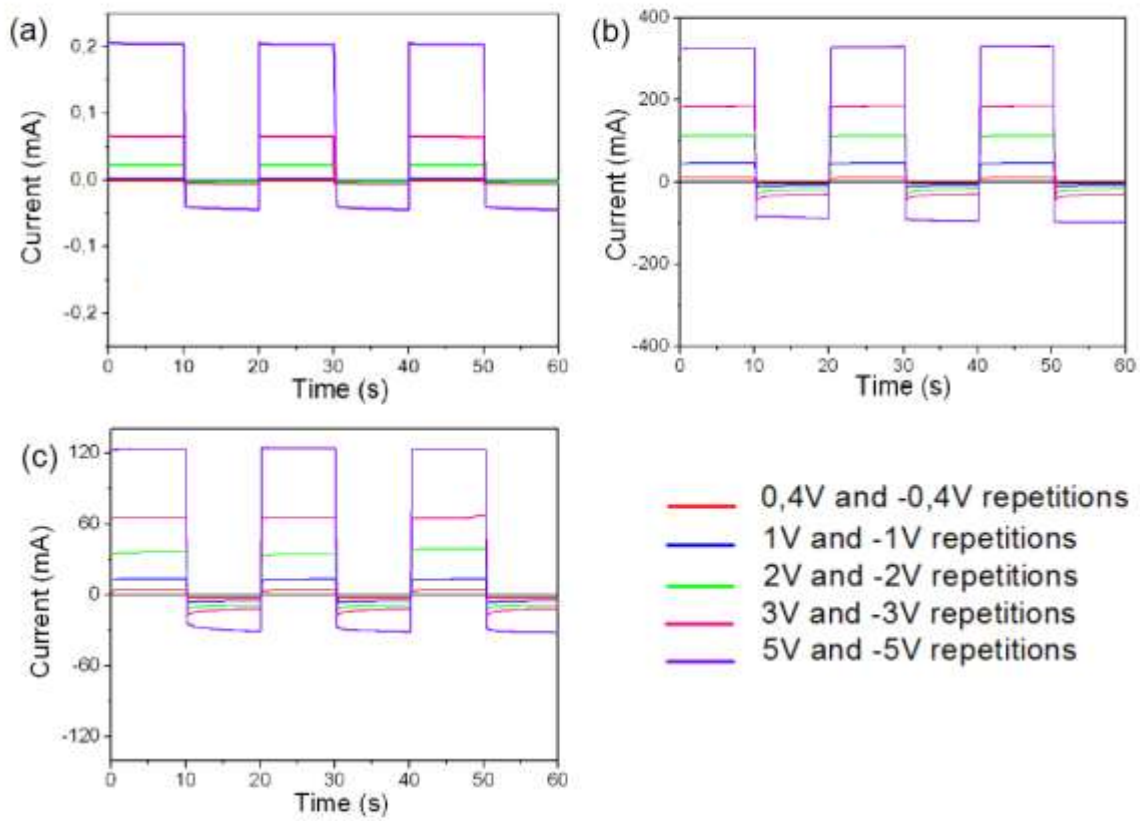

Figure 7. Rectification properties of porous GaN diodes formed by (a) an undoped *n*-type porous GaN layer grown on the top a non-porous *p*-type GaN substrate, (b) a Mg-doped porous *p*-type GaN layer grown on a non-porous *n*-type GaN substrate, and (c) a Mg-doped porous *p*-type GaN layer grown on an undoped porous *n*-type GaN film previously grown on a non-porous *n*-type GaN substrate.

Porous GaN MOS diodes fabricated by CVD

By increasing the concentration of Mg_3N_2 in the synthesis of porous GaN we have discovered the possibility of fabricating MgO-GaN metal-oxide semiconductor (MOS) diodes in one single synthesis step (26). The synthesis consisted in using a molar ratio Mg/Ga = 0.052, locating the Mg_3N_2 precursor of Mg 4 cm upstream of the Ga source. In this case, Si (100) substrates were used, coated with a thin catalyst layer 20 nm thick of Pt or Au to facilitate the nucleation of the porous GaN particles (24). Under these conditions, a layer of crystalline MgO was formed underneath the Mg-doped GaN layer.

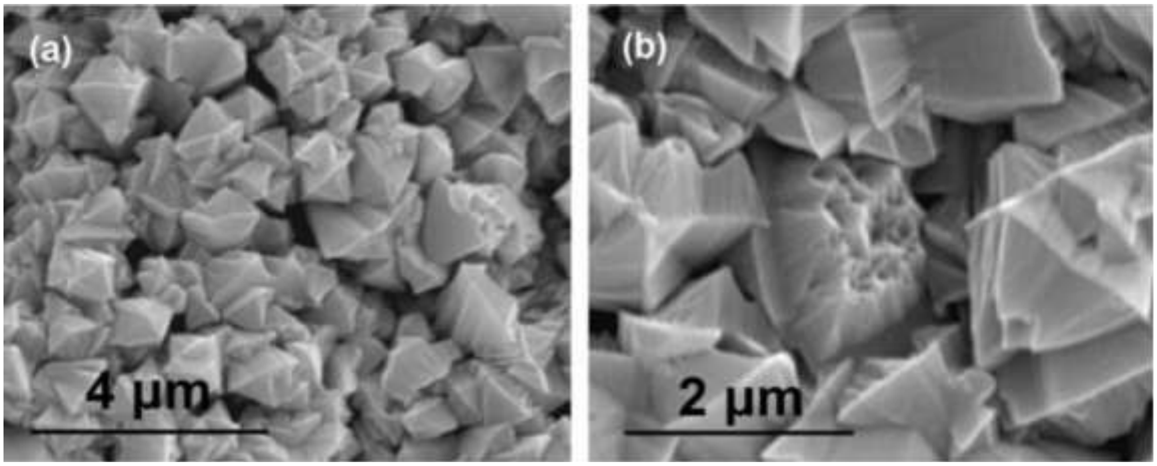

Figure 8. SEM image of the porous GaN particles nucleated on the top of the MOS structure grown on Si (100) substrates coated with (a) a 20 nm thick film of Au and (b) a 20 nm thick film of Pt.

Figure 8 shows the characteristic morphology of the porous GaN particles, with a mean size of ~1.5 μm, that nucleated on the top of the MOS structure. In this figure it can be clearly seen the intraparticle and the interparticle porosity, typical of these structures.

The XRD pattern of the MOS diode, shown in Figure 9 shows the presence of polycrystalline wurtzite GaN, as well as MgO on these structures. Even, the peak corresponding to the Si substrate can be seen in this figure.

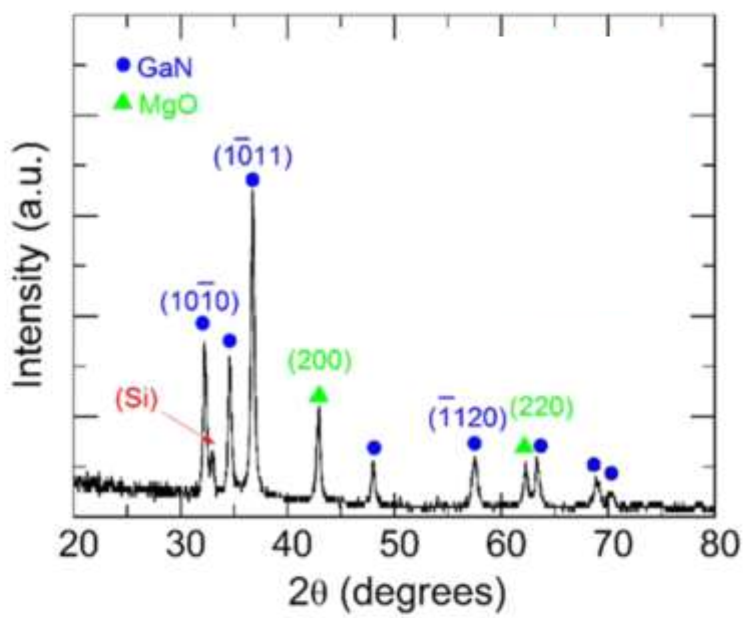

Figure 9. XRD pattern of the porous MgO-GaN MOS structure grown on a Si (100) substrate.

The combination of cross-section TEM images and energy dispersive X-ray spectrometry (EDX) analysis allowed determine the location of the MgO layer in the structure, just underneath the porous GaN polycrystalline layer (see Figure 10). The TEM image reveals the presence of different regions with a variation in contrast, corresponding to the different Mg concentration. Through the quantification of the Mg concentration by EDX, four different spatial regions could be defined in the sample: (i) a region corresponding to the Si substrate; (ii) a second region (corresponding to point 1 in Figure 10) corresponding to the formation of an intermetallic Mg-Ga (27 % - 73 %) alloy; (iii) a third layer in which MgO is encountered (corresponding to points 2-4 in Figure 10); and (iv) the Mg-doped GaN layer (corresponding to points 5-12 in Figure 10).

The electrical characterization of the MgO-GaN porous layers formed on silicon exhibit a diode behavior which is consistent with a MOS system. The I-V curves recorded, plotted in Figure 11 (a), show a rectifying diode response. We assumed that the net current is due to the thermionic emission current, as the metal-semiconductor-metal contact now involves a dielectric on one interface, mimicking the structure of a Schottky contact with series resistances originated from the MgO and porous *n*-type GaN. We believe that effective Ohmic contacts can form with *n*-type GaN suggesting that Ohmic transport is dominated by resistivity through the Mg-Ga alloy interface. However, when the MgO layer is introduced, since it has a high dielectric constant, the series resistance increase in an important way even at low voltages. Thus, the system exhibit a diode behavior but utilizing an Ohmic contact formed by the Mg-Ga intermetallic found under the MgO layer and biased by the underlying Si substrate. The series resistance, however, seems to include also tunneling effects (such as Poole-Frenkel tunneling and surface leakage), since the ideality factor depends strongly on the voltage, becoming quite high in the region corresponding to high current and high voltage, as plotted in Figure 11 (b).

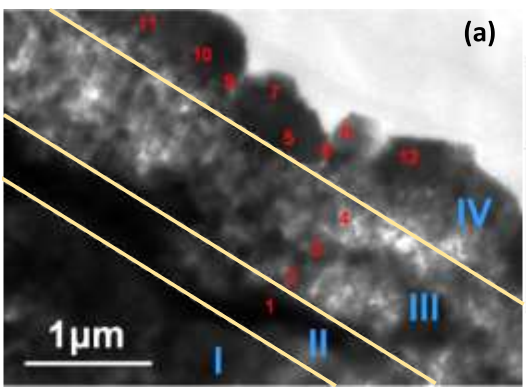

(b)

Position #	Mg %	Ga %	Position #	Mg %	Ga %
1	73.3	26.7	7	11.7	97.8
2	98.5	1.5	8	7.9	92.1
3	97.0	3	9	9.5	90.5
4	97.3	2.7	10	8.9	91.1
5	7.9	92.1	11	7.9	92.1
6	11	89	12	8.1	91.9

Figure 10. (a) Cross-section TEM image of the porous MgO-GaN MOS diode fabricated by CVD in a single synthesis step on a Si (100) substrate, and (b) EDX content of Mg and Ga identified in the different layers of the structure.

This method of fabrication of MOS diodes in a single synthesis step might be extended to growing nanoscale III-N materials and alloys using metals that are not typically employed for forming electric contacts, to provide an Ohmic response and fabricate MOS-based systems to be used in high surface area transistors for biosensing applications that are chemically stable.

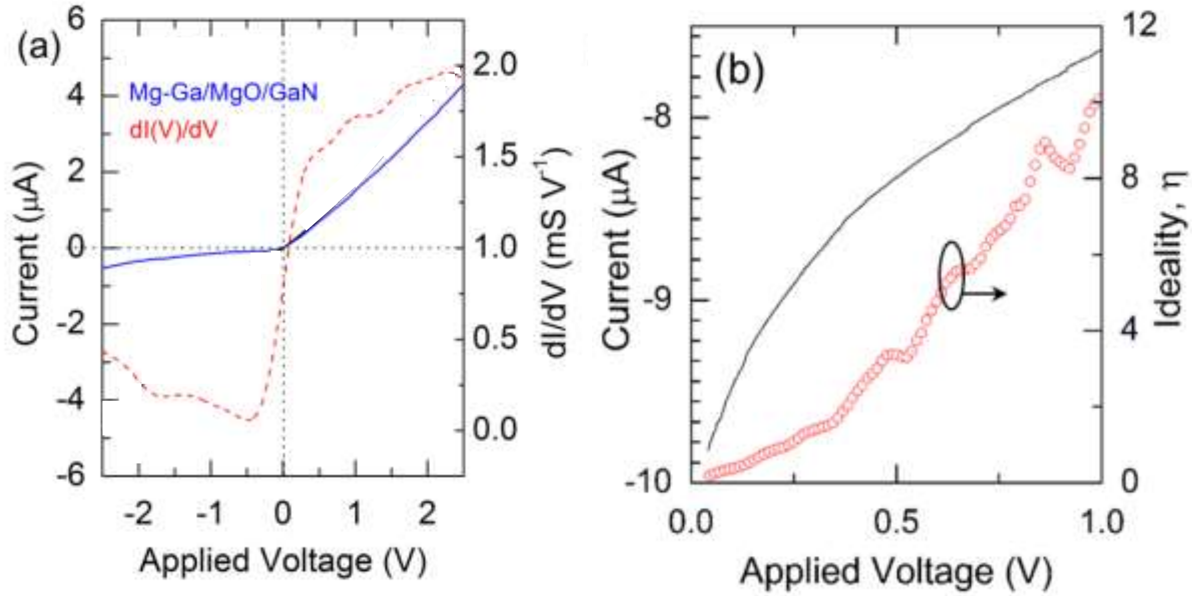

Figure 11. (a) I-V curves for porous *n*-type GaN with a MgO dielectric layer underneath. (b) ln(I)-V curve and the voltage dependence of the ideality factor for the diode.

An approximation towards the fabrication of porous GaN LEDs produced by CVD

To explore the possibility of fabricating LEDs based on porous GaN produced by CVD we used the diodes formed by an *n*-type porous GaN layer deposited on a *p*-type non-porous GaN substrate, described above (28).

These structures were characterized as LEDs by injecting current by a two probes measurement system that allowed stablishing contacts on the top of the substrate and on the top of the porous GaN layer, using a Keithley 2400 sourcemeter. To ensure a good electrical contact on the sample, especially on the rough surface of the porous substrate, In/Ga liquid drops were deposited on the top of the substrate and the porous GaN layer to obtain a good wetting, in which the needles of the two probes measurement systems were introduced. At the same time, the use of this liquid alloy allowed to generate an Ohmic contact on both sides of the diode.

Figure 12 (a) shows the optical image taken showing the electroluminescence (EL) generated by these devices at 100 mA. It can be seen that light blue light is generated by these kind of structures. Since no electrodes were deposited covering the whole surface of the sample, the light arises only from the point where the contact was stablished, thus it is emitted from a narrow area of the device.

Figure 12 (b) shows the EL spectra of these light blue LEDs at the injection currents from 24 to 100 mA. The first important thing to note here are the high voltages that we needed to apply to obtain these injection currents. This is due to the high resistivity of the substrates used. The emission spectra consists of only one peak. At low injection currents (24-50 mA), this peak is very broad, with very low intensity, centered at around 542 nm. It is not until we applied 66 mA that the emission peak is clearly defined, centered at ~521 nm. This corresponds to a voltage of 13 V that seems to be the turn on voltage for these structures. As the injection current increases, the emission peak shifts towards shorter wavelengths, and it becomes centered at 500 nm for an injection current of 100 mA. The full width at half maximum (FWHM) of this emission peak also becomes narrower as the injection current increases, passing from 103 nm at 66 mA to 77 nm at 100 mA.

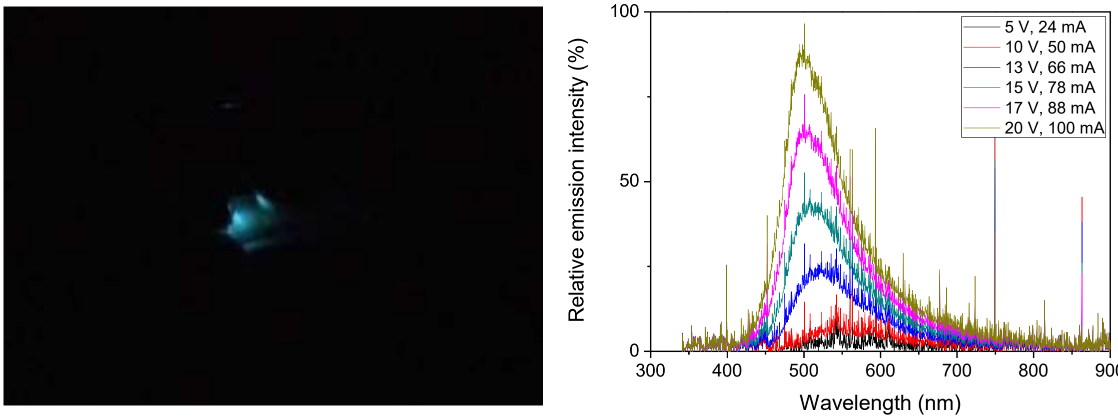

Figure 12. (a) Optical image of the emission generated, and (b) room temperature electroluminescence spectra of the LEDs based on an *n*-type porous GaN layer deposited on a *p*-type non-porous GaN substrate.

Despite the voltages we need to apply to obtain light from these structures are still very high, we are optimistic that by selecting non-porous GaN substrates with lower resistivity, we would be able to reduce the turn on voltage for these LEDs. Also, we observed that even if we increase the injection current of the LED to the point in which we cause the rupture of the diode and the emission of the device is stopped, by moving the top contact to another point of the surface of the porous layer, we can obtain again the emission. This would indicate that the epitaxial layer consists on a grain structure. Thus, here, the resistance generated at the grain boundaries might also play a role in the high turn on voltages obtained. Nevertheless, the grain structure of the LED might be seen as an advantage since it would be formed by a multitude of tiny diode structures connected among them in parallel. Thus, the failure or the rupture of the Schottky diode would not cause the failure of the whole system.

Conclusions

In this paper, we reviewed the potentiality of porous GaN produced by CVD to fabricate *p*-*n* junction rectifiers, MOS diodes and LEDs deposited by a simple synthesis method on large substrate areas. The results reviewed here, taken as a whole, demonstrate that high quality *p*-*n* junctions of porous *n*-type and porous *p*-type GaN can be obtained by chemical vapor deposition. The electrical characteristics demonstrate the high electronic quality of the produced porous GaN layers.

We believe that these kind of structures can be extended to other III-N materials such as InN and AlN as a route toward porous and graded index III-N materials that constitute a basis for the development of white light emitting LEDs with reduced reflection losses and narrowed output light cones that might improve their external quantum efficiencies, among other applications.

Acknowledgments

This work was supported by the Spanish Government under projects TEC2014-55948-R and Mineco/AEI/FEDER MAT2016-75716-C2-1-R and the Catalan Authority under project 2014SGR1358. FD acknowledges additional support through the ICREA Academia awards 2010ICREA-02 for excellence in research.

References

1. Y. Zhang, B. Leung, J. Han, *Appl. Phys. Lett.*, **100**, 181908 (2012).
2. S. Nakamura, M.R. Krames, *Proc. IEEE*, **101**, 2211 (2013).
3. S.C. Jain, M. Willander, J. Narayan, R.V. Overstraeten, *J. Appl. Phys.*, **87**, 965 (2000).
4. H. Shibata, Y. Waseda, H. Ohta, K. Kiyomi, K. Shimoyama, K. Fujito, H. Nagaoka, Y. Kagamitani, R. Simura, T. Fukuda, *Mater. Trans.*, **48**, 2782 (2007).
5. R. Dahal, B. Pantha, J. Li, J.Y. Lin, H.X. Jiang, *Appl. Phys. Lett.*, **94**, 063505 (2009).
6. C.J. Neufeld, N.G. Toledo, S.C. Cruz, M. Iza, S.P. DenBaars, U.K. Mishra, *Appl. Phys. Lett.*, **93**, 143502 (2008).
7. J.J. Wierer, A. David, M.M. Megens, *Nat. Photon.*, **3**, 163 (2009).
8. J.C. Vial, A. Bsiesy, F. Gaspard, R. Herino, M. Ligeon, F. Müller, R. Romestain, R.M. Macfarlane, *Phys. Rev. B*, **45**, 14171 (1992).
9. J.M. Hwang, W.H. Hung, H.L. Hwang, *IEEE Photon. Technol. Lett.*, **20**, 608 (2008).
10. R. Wang, D. Liu, Z. Zuo, Q. Yu, Z. Feng, X. Xu, *AIP Adv.*, **2**, 012109 (2012).
11. K. Kim, J. Choi, T.S. Bae, M. Jung, D.H. Woo, *Jpn. J. Appl. Phys.*, **46**, 6682 (2007).
12. S.W. Ryu, J. Park, J.K. Oh, D.H. Long, K.W. Kwon, Y.H. Kim, J.K. Lee, J.H. Kim, *Adv. Funct. Mater.*, **19**, 1650 (2009).
13. C.Y. Cho, S.E. Kang, K.S. Kim, S.J. Lee, Y.S. Choi, S.H. Han, G.Y. Jung, S.J. Park, *Appl. Phys. Lett.*, **96**, 181110 (2010).
14. S. Chhajed, W. Lee, J. Cho, E.F. Schubert, J.K. Kin, *Appl. Phys. Lett.*, **98**, 071102 (2011).
15. X. Fu, B. Zhang, X. Kang, J. Deng, C. Xiong, T. Dai, X. Jiang, T. Yu, Z. Chen, G.Y. Zhang, *Opt. Express*, **19**, A1104 (2011).
16. A. Ramizy, Z. Hassan, K. Omar, *Sens. Actuators B*, **155**, 699 (2011).
17. F.K. Yam, Z. Hassan, *Appl. Surf. Sci.*, **253**, 9525 (2007).
18. J. Mena, J.J. Carvajal, O. Martínez Sacristan, J. Jimenez, V.Z. Zubialevich, P.J. Parbrook, F. Díaz, M. Aguiló, Nanotechnol. (2017)
19. A.P. Vajpeyi, S.J. Chua, S. Tripathy, E.A. Fitzgerald, W. Liu, P. Chen, L.S. Wang, *Electrochem. Solid-State Lett.*, **8**, G85 (2005).
20. M. Ohkubo, *J. Cryst. Growth*, **189-190**, 734 (1998).
21. D.J. Díaz, T.L. Williamson, I. Adesida, P.W. Bohn, R.J. Molnar, *J. Appl. Phys.*, **94**, 7526 (2003).
22. C. Youtsey, I. Adesida, G. Bulman, *Appl. Phys. Lett.*, **71**, 2151 (1997).
23. J.J. Carvajal, J.C. Rojo, *Cryst. Growth Des.*, **9**, 320 (2009).
24. O.V. Bilousov, J.J. Carvajal, D. Drouin, X. Mateos, F. Díaz, M. Aguiló, C. O'Dwyer, *ACS Appl. Mater. Interfaces*, **4**, 6927 (2012).

25. O.V. Bilousov, H. Geaney, J.J. Carvajal, V.Z. Zubialevich, P.J. Parbrook, A. Giguère, D. Drouin, F. Díaz, M. Aguiló, C. O'Dwyer, *Appl. Phys. Lett.*, **103**, 112103 (2013).
26. O.V. Bilousov, J.J. Carvajal, A. Vilalta-Clemente, P. Ruterana, F. Díaz, M. Aguiló, C. O'Dwyer, *Chem. Mater.*, **26**, 1243 (2014).
27. O.V. Bilousov, J.J. Carvajal, J. Mena, O. Martínez, J. Jiménez, H. Geaney, F. Díaz, M. Aguiló, C. O'Dwyer, *CrystEngComm*, **16**, 10255 (2014).
28. O.V. Bilousov, J.J. Carvajal, H. Geaney, V.Z. Zubialevich, P.J. Parbrook, O. Martínez, J. Jiménez, F. Díaz, M. Aguiló, C. O'Dwyer, *ACS Appl. Mater. Interfaces*, **6**, 17954 (2014).
29. J.J. Carvajal, J. Mena, O.V. Bilousov, O. Martínez, J. Jiménez, V.Z. Zubialevich, P.J. Parbrook, H. Geaney, C. O'Dwyer, F. Díaz, M. Aguiló, *ECS Trans.*, **66**, 163 (2015).
30. O.V. Bilousov, J.J. Carvajal, D. Drouin, A. Vilalta, P. Ruterana, M.C. Pujol, X. Mateos, F. Díaz, M. Aguiló, C. O'Dwyer, *ECS Trans.*, **53**, 17 (2013).
31. Y.T. Moon, Y. Fu, F. Yun, S. Dogan, M. Mikkelson, D. Johnstone, H. Morkoç, *Physica Status Solidi A*, **202**, 718 (2005).
32. S.J. Pearton, R.G. Wilson, J.M. Zavada, J. Han, R.J. Shul, *Appl. Phys. Lett.*, **73**, 1877 (1998).